Nanoscale

PAPER

3D branched nanowire heterojunction photoelectrodes for high-efficiency solar water splitting and H_2 generation†

Ke Sun,[a] Yi Jing,[a] Chun Li,‡[ab] Xiaofeng Zhang,[c] Ryan Aguinaldo,[a] Alireza Kargar,[a] Kristian Madsen,[a] Khaleda Banu,[a] Yuchun Zhou,[a] Yoshio Bando,[b] Zhaowei Liu[a] and Deli Wang*[ade]

We report the fabrication of a three dimensional branched ZnO/Si heterojunction nanowire array by a two-step, wafer-scale, low-cost, solution etching/growth method and its use as photoelectrode in a photoelectrochemical cell for high efficiency solar powered water splitting. Specifically, we demonstrate that the branched nanowire heterojunction photoelectrode offers improved light absorption, increased photocurrent generation due to the effective charge separation in Si nanowire backbones and ZnO nanowire branching, and enhanced gas evolution kinetics because of the dramatically increased surface area and decreased radius of curvature. The branching nanowire heterostructures offer direct functional integration of different materials for high efficiency water photoelectrolysis and scalable photoelectrodes for clean hydrogen fuel generation.

Introduction

Currently over 90% of electricity and over 95% of hydrogen are produced from fossil fuels and biomass.[1] Fossil fuels are believed to be the major cause of negative and irreversible environmental consequences,[2] which contribute the largest amount of greenhouse gas (carbon dioxide)[3,4] and air pollution (nitrous oxide and smog). Hydrogen is believed to be one of the sustainable and clean-energy alternatives to overcome the environmental challenges, which can work by itself as a source of energy or together with other carbon source to generate liquid hydrocarbons.[5] In order to be economically competitive and environmentally beneficial, it is essential to find a cost-effective and clean method for mass production of hydrogen.[6] Techniques for directly converting water to hydrogen using solar energy, known as photoelectrolysis, are receiving great attention recently, despite the fact

that the electrolysis effect was discovered more than 200 years ago.[7] Mechanisms of water splitting driven by semiconductor photoelectrochemical (PEC) electrodes (photoelectrodes) are depicted in previous review works.[8–11] Continuous research effort and current challenges are to optimize photoelectrodes towards practical PEC applications with a broad spectrum of absorption, matching energy band to water reduction/oxidation energy levels, long-term stability in harsh conditions (like seawater or effluent, under both dark and illumination conditions), and most importantly high photocurrent density in order to reach high photo-to-hydrogen conversion efficiency.[12]

Materials that are currently attracting research interests include semiconductors (Si,[13–15] III–V,[16,17] II–VI,[18–21] *etc.*) and metal oxides (TiO$_2$,[22] ZnO,[23] Fe$_2$O$_3$,[24–26] WO$_3$[27–29]). Moreover, using heterojunction[30–33] or homojunction[34,35] and tandem cells enhances light absorption, charge separation and appropriate carrier energy, all of which could lead to a potentially viable device for spontaneous water splitting. Among all of the aforementioned materials, Si as one of the cheapest, most abundant, and most important semiconductor materials, has demonstrated broad application as solid-state solar cells and PEC cell devices. Recently, a one-dimensional nanowire (NW) array utilized in a Si solar cell provides conceptual advantages, such as improved light absorption and potentially improved charge separation.[13,36–40] On the other hand, Si nanostructure based photoelectrodes interfacing with liquid electrolyte as an alternative format of solar cells have shown great potential due to the advantages of high quality and conformal junction interface. Meanwhile, this structure improves the junction area, essentially eases the carrier separation and collection. Previously studies have demonstrated photoelectrodes with improved PEC properties using a p-type[14,41] or an n-type[31,42] doped Si NW array as

[a]Department of Electrical and Computer Engineering, University of California, San Diego 9500 Gilman Drive, La Jolla, CA, 92093, USA. E-mail: dwang@ece.ucsd.edu
[b]International Center for Materials Nanoarchitectonics (MANA), National Institute for Material Science, Namiki 1-1, Tsukuba, Ibaraki 305-0044, Japan
[c]Changchun Institute of Applied Chemistry, Chinese Academy of Sciences, 109 Remin Street, Changchun, Jilin, 130021, China
[d]Materials Science and Engineering, University of California, San Diego 9500 Gilman Drive, La Jolla, CA, 92093, USA
[e]California Institute of Telecommunication and Information Technology, University of California, San Diego 9500 Gilman Dr, La Jolla, CA, 92093, USA
† This article was submitted as part of a collection highlighting papers on the 'Recent Advances in Semiconductor Nanowires Research' from ICMAT 2011.
‡ Current address: Materials Science and Engineering, North Carolina State University, 911 Partner's Way, Raleigh, NC, 27607, USA.

a photocathode or a photoanode, respectively. A large surface area provides significantly increased photoelectrochemical sites for water reduction/oxidation. However, problems with NW structures happen at the electrolyte interfaces where increased surface state recombination occurs. Moreover, poor interface kinetics further limits the performance of Si based photo-electrodes, resulting in low H_2 evolution.[43,44] In this article, we present a low-cost two-step solution phase integration of ZnO NW branches to Si NW backbones and the use of these p/n branched heterostructures for solar water splitting. The branched NW array structure is studied using scanning electron microscopy (SEM) and high-resolution transmission electron microscopy (HR-TEM). Structures with different lengths of Si NW backbones and ZnO NW branches are studied as a photo-cathode for H_2 production. Light absorption and transient current density at chopped light are studied.

Experimental

1. Device fabrication

p-Type boron doped (111) silicon wafers with a thickness of 250 μm (WaferWorld 1–10 Ω cm) were cleaned with solvent, rinsed with deionized (DI) water (>17.8 MΩ cm) and dried with N_2. The metal assisted chemical etching used to prepare the Si NW substrate is described in previous literatures[45–47] and as follows: a cleaned 2″ wafer, with both the edge and backside protected from exposure to the solution with polymer coating, was fixed on a homemade etching setup and immersed in the etching solution (a mixture of 0.02 M $AgNO_3$ and 4 M HF in DI water). The etching was performed at 50 °C with gentle agitation (100 rpm) for varying time periods, followed by immediate removal from the etching solution and thorough rinse with DI water for 5 min. The as-etched Si NWs were normally coated with a thick layer of chemically reduced Ag, the latter was etched in dilute nitric acid (1 : 10) for at least 1 h (depending on the length of NW). Finally, samples were rinsed well in DI water and dried gently with N_2.

For ZnO nanowire growth, a thin ZnO seeding layer was deposited on the Si NW substrates with low-pressure argon plasma RF sputtering using 99.99% ZnO target. Prior to the seeding process, Si NW samples were dipped in buffered oxide etching (1 : 6 BOE) solution for 10 s to remove the native oxide. Then, samples were carefully spray-cleaned using DI water, dried with N_2, and immediately transferred to a deposition chamber to minimize oxidation. During the sputtering, pressure in the chamber was maintained at 1.7 mTorr. The deposition rate was first characterized on a planar Si substrate. A thin layer of ZnO with 45 nm in thickness was achieved after 16 min, based on the deposition rate calculated from thin film deposition on the planar Si substrate. Hydrothermal growth of ZnO NWs[48,49] was carried out as follows: Si substrates were fixed on a supporting glass slide facing down and immersed in the reaction solution—25 mM solutions of zinc acetate and hexamethylenetetramine (HMTA, Sigma) in DI water at 85 °C with gentle agitation for varying time periods. The as-grown samples were ultrasonicated at low power (<30 W) to remove ZnO particles on the surface, thoroughly rinsed with DI water, and gently blow-dried with N_2 gas. Samples were stored under vacuum to minimize oxygen and water absorption before further measurement.

2. Morphological study

The NW morphology was examined using a field emission secondary electron microscope (FESEM, FEI-XL30) with an accelerating voltage of 5.0 kV. Energy dispersive X-ray (EDX) analysis was used to examine the efficiency of Ag etching. A cross-sectional transmission electron microscope (XTEM, JEOL JEM-3100FEF) equipped with an OMEGA-type energy filter in the microscope column with an accelerating voltage of 300 kV was used to study the crystalline structures and the ZnO/Si heterostructure interfaces. Images were collected using the Gatan image recording system with a resolution of 0.5 nm.

3. Reflectance measurement

Optical extinction spectra were measured using a halogen lamp and a CCD spectroscope coupled with an optical microscope.[50] Samples are in focus of microscope objectives. Specular and diffuse scattered light from the sample were collected using 50× objective lens (Carl Zeiss 422370-9960-000) with a numerical aperture of 0.8 and working distance of 0.6 mm. Reflected light was measured using a CCD spectrometer (Andor Shamrock). The diameter of the effective field of view collected by the CCD was around 50 μm.

4. PEC measurement

Prior to PEC measurement, indium paste was applied at the back of the sample and a copper wire was soldered to the sample providing ohmic electrical contacts. The backside and edges of samples were protected using epoxy and the copper wire was sealed in plastic tubes to prevent electrical shorts to the electrolyte such that only the sample front side was in contact with the electrolyte. Si NWs without ZnO NW branches were etched for 10 seconds in HF solution at room temperature and rinsed with DI water immediately prior to measurement, the ZnO/Si branched NW samples were tested directly without further treatment. The area of the samples exposed to the electrolyte varies and ranges about 0.5–1.2 cm². In electrochemical measurement using one-compartment cell setup, Pt wire was used as the counter electrode (CE) and was positioned as close as possible to the photocathode, while the Ag/AgCl (1 M KCl) reference electrode (RE) was placed as close as possible to the photocathode working electrode (WE). A xenon lamp from a solar simulator providing an output light intensity of 130 mW cm^{-2} was incident normal to the sample through a quartz window. Steady-state photocurrent density–voltage ($J–V$) curves under a slow scan rate (5 mV s^{-1}), and photocurrent density–time ($J–t$) curves were obtained by using a potentiostat (Digi-Ivy Inc). All data were recorded using software DY2300. The electrolyte solution was always 400 ml of 0.25 M Na_2SO_4 buffered with PBS with pH ≈ 7.2, which was measured using a pH meter (Acorn-Oakton pH5).

Results and discussions

Fig. 1 shows the cross-sectional and top views of Si/ZnO branched NW arrays with different backbone and branched lengths. Similar to the growth on the plain Si substrate, hexagonal ZnO NWs grown on the surface of Si NW backbones were
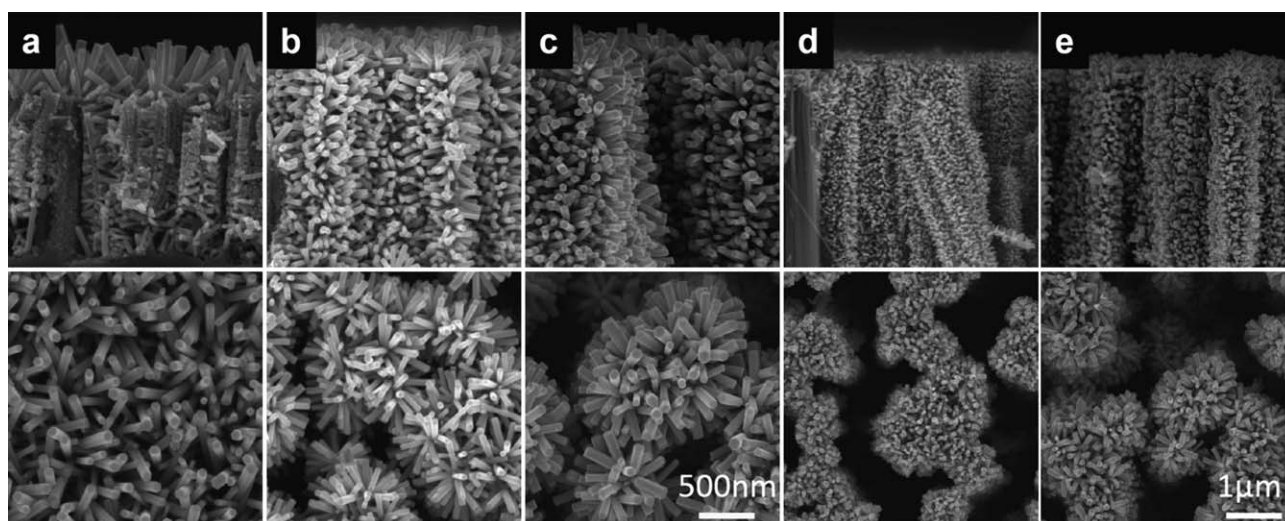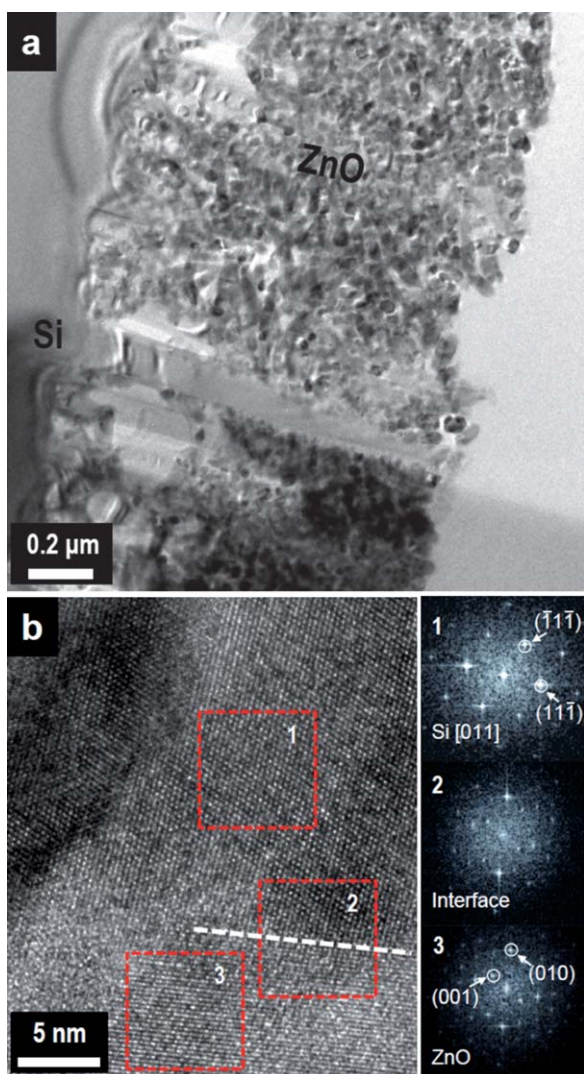
Fig. 1 Cross-sectional view (top row) and top view (bottom row) SEM images of Si/ZnO branched NW arrays with different backbone and branch lengths. ZnO NW branches from growth for 2.5 h on Si NWs with different lengths by chemical etching for (a) 5 min, (b) 10 min, and (c) 15 min, respectively (scale bar = 500 nm). ZnO NW branches grown for various times of (d) 30 min and (e) 2.5 h on Si NW arrays etched for 15 min (scale bar = 1 μm).

nearly perpendicular.[51] Geometries, distributions, and even optical properties of the ZnO branches strongly depend on the Si NW array. ZnO NW branches grown on short Si NWs (5 min etching) showed position-dependent sizes: ZnO NWs on the sidewall were smaller in both the diameter and length than those growing on top of the Si NW array (Fig. 1a). The position-dependent non-uniformity of ZnO NW growth is believed to be due to the limited diffusion of ZnO nanoparticles (NPs) during the hydrothermal growth from the reaction solution to nucleation sites on the sidewalls of the Si NWs. However, better uniformity was reached when ZnO NW branches grow on longer Si NWs (10 and 15 min etching), as shown in Fig. 1b and c. Longer Si NWs give smaller moments of inertia and spring constants; therefore they are more flexible, allowing van der Waals forces to deform adjacent NWs into clusters, which consequently affect the overall optical and electrical properties. This will be discussed in detail in later sections. Collapsed long NWs leave wider openings and thus ease the diffusion of ZnO NPs, which results in a uniform growth independent of the position. Moreover, ZnO NW branches grown on the same Si NW substrate for varying amounts of time are shown in Fig. 1d and e. Shorter and thinner branches were realized from 30 min growth (Fig. 1d), while branches were longer and wider in the case of 2.5 h growth (Fig. 1e). Estimation showed the extraordinary high density of ZnO NWs in the highly ordered 3D branched NW array. Techniques used for etching Si NW and growth of ZnO NW provided the advantages and potential applications in large-scale fabrications and cost-effective solution phase integration of nanoscale heterojunctions.

Fig. 2 shows TEM images of the branched NW sample fabricated on 5 min etched Si NW array. The cross-sectional TEM image at low magnification in Fig. 2a illustrated the non-uniform distribution of ZnO NWs on Si NWs, which may be due to the non-uniformity of Si NW diameters (20–200 nm) from the wet etching and the uneven coating of a ZnO seeding layer from RF magnetron sputtering. Secondly, samples could be slightly

damaged during the TEM sample preparation process using the focus ion beam (FIB) milling. It can be seen from the high resolution TEM image (Fig. 2b) that there is no noticeable amorphous SiO_x at the ZnO/Si interface, even for samples that were stored in air for days prior to the TEM characterization. We believe that this is due to the HF etching, prior to sputtering of the ZnO seeding layer. H-terminated Si NW surfaces were effectively generated which made the Si NWs less prone to oxidation.[52] On the other hand, the interfacial native oxide layer as one kind of passivation layers could also benefit the device performance and its effect on optoelectrical properties was discussed before.[53–55] In our experiments, the rough surface of solution etched Si NWs provided high density of nucleation sites during the seeding layer deposition, which in turn promoted the growth of ZnO NW branches in the high aspect ratio Si NW arrays.
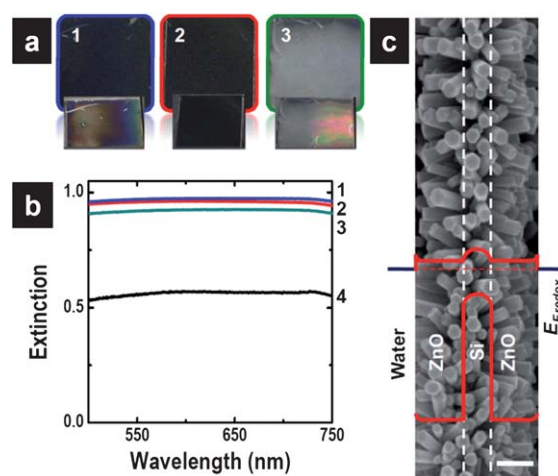
The wet-etched Si NW samples were dark and discoloration was observed after the growth of ZnO NW branches. Extinction spectra in the visible range (500–750 nm, which was limited by the optics of the measurement setup) were measured using a microscope with samples in focus and a CCD spectrometer (measurement setup details can be found in supporting document). Extinction spectra and optical images of different samples with the same Si NW length but different ZnO NW lengths are shown in Fig. 3. The Si NW sample etched for 5 min showed excellent and uniform light absorption around 95% (Fig. 3a-2 and red curve in Fig. 3b). This was due to the aperiodic and sharp-tip structure of the etched Si NW, which in turn smoothed the transition of refractive index of air to that of Si substrate[56] and also suppressed the angle of incident (AOI) effect.[41,57] Short time (30 min) growth of ZnO NW on Si NW (Fig. 3a-1 and blue curve in Fig. 3b) showed improved light absorption (up to 97.5%). This is believed to be due to the filling of ZnO ($n_{ZnO} = 1.94$–2.4)[58,59] in between Si NWs ($n_{Si} = 3.54$–6.8)[60] in the wavelength range 240–1100 nm further smoothening the refractive index transition from light incident media ($n_{air} = 1$) to the Si

Fig. 2 TEM images of ZnO/Si branched NW arrays: (a) low resolution TEM showing the branched structure, (b) high-resolution TEM showing the interface of a typical single ZnO NW branch or a seeding particle on the surface of Si NWs. Insets are fast Fourier transform (FFT) patterns of the corresponding areas in (b).

Fig. 3 (a) Optical images (first row: top view and second row: ~45 degree view) and (b) extinction spectra of different substrates: (1) 0.5 h ZnO NW growth on 5 min etched Si NW array (dark black, blue cure), (2) 5 min as-etched Si NW array (dark brownish, red curve), and (3) 2.5 h ZnO NW growth on 5 min etched Si NW array (light gray, green curve), and (4) polished Si reference sample (black curve). Sample size in this experiment is kept at 0.5×0.5 in². (c) Single Si/ZnO branched NW interfacing with the electrolyte superimposed with the energy band diagram at zero external bias with light illumination (scale bar = 200 nm).

ZnO is lower than that of Si, which assists photo-generated electrons to transfer across the ZnO layer to the water reduction level, whereas holes flow to the back contact of Si. Band bending and an electron barrier at the ZnO/electrolyte interface due to the interaction with oxygen and water were also illustrated, which, we believe, is very important to the understanding of device performances. In addition, trapped O_2[62] on the ZnO NW surface results in a higher electron barrier at the electrolyte/ZnO interface, and thus a high onset potential. Branched NWs also offer other additional advantages as photoelectrodes in photoelectrochemical cells such as large surface area and large surface curvature leading to enhanced surface chemical reaction and more efficient H_2 evolution. Fig. 4a shows the J–V characteristics of the ZnO/Si branched NWs with different Si NW lengths. The longer Si NWs (from 15 min etching) give 50–100% higher photocurrent compared to that of the 5 min etched sample, which is believed to be due to the enhancement of light absorption and the larger overall surface area of the ZnO branches. Note that the dark current from the 15 min etched sample is much larger than the 5 min etched sample (Fig. 4a, inset), due to the much increased junction and surface area and thus recombination centers. Significant photocurrent was noticed starting at −1 V external potential and H_2 evolution was easily observed with the naked eyes in both samples (Fig. 4c). No photocurrent plateaus were observed indicating no light intensity limited photocurrent at the potential range measured.

Fig. 4b and the inset compare the current density from the branched NW photoelectrodes with different lengths of ZnO NW branches but the same Si NW length (etched for 5 min). The electrodes tested are 5 min etched Si NWs coated with the ZnO seeding layer, ZnO NWs grown for 30 min and 2.5 h, respectively. The photocathodic currents turn on at around −1 V and increase with the applied negative bias for the branched NW

substrate. However, the AOI effect became worse in ZnO NW branched samples (Fig. 3a). This can be seen in Fig. 3a where the optical image taken from a 45 degree viewing angle (second row) revealed the reflection patterns on this sample. Furthermore, the sample with longer ZnO NW branches (green curve in Fig. 3b) did not show further improvement in the light absorption. Careful investigation under SEM showed a more disordered structure of ZnO NWs from longer growth time, which scatters more light resulting in a light gray color (Fig. 3a-3). Therefore, we can conclude that the light absorption enhancement by vertical NW arrays minimizing light reflection/scattering is a combination effect of NW size, density, and shape.[61]
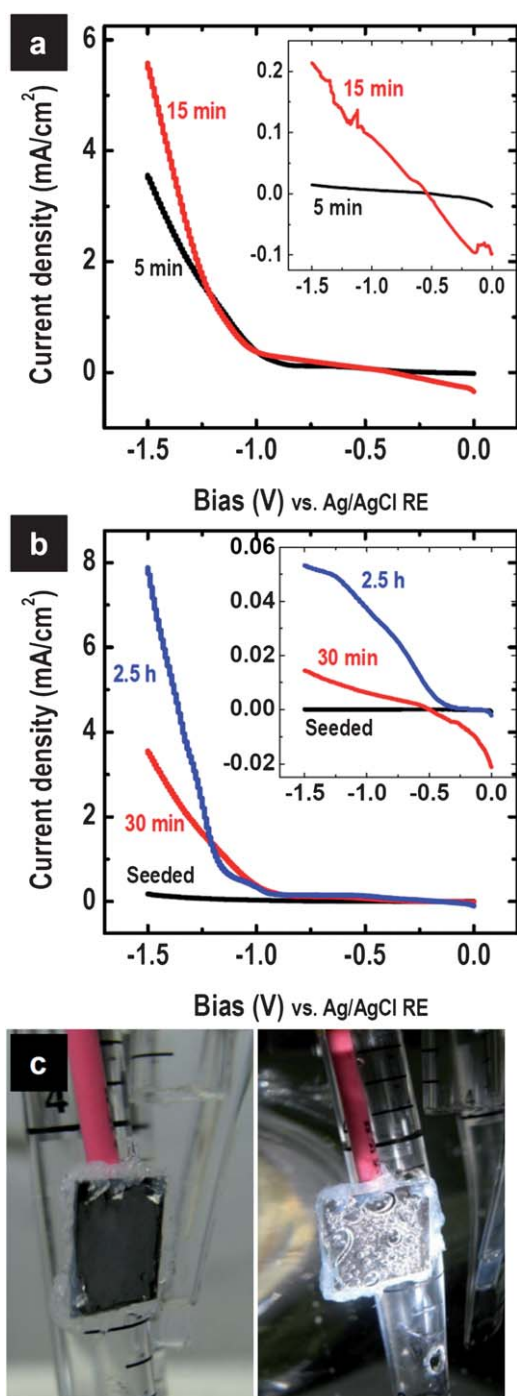
Fig. 3c shows the SEM image of ZnO NWs (branches grown on a single Si NW backbone) superimposed with the energy band diagram and water reduction level (at pH = 7). Si NWs with diameters larger than 20 nm were assumed to have the same electronic band gap as the bulk Si.[52] The conduction band of
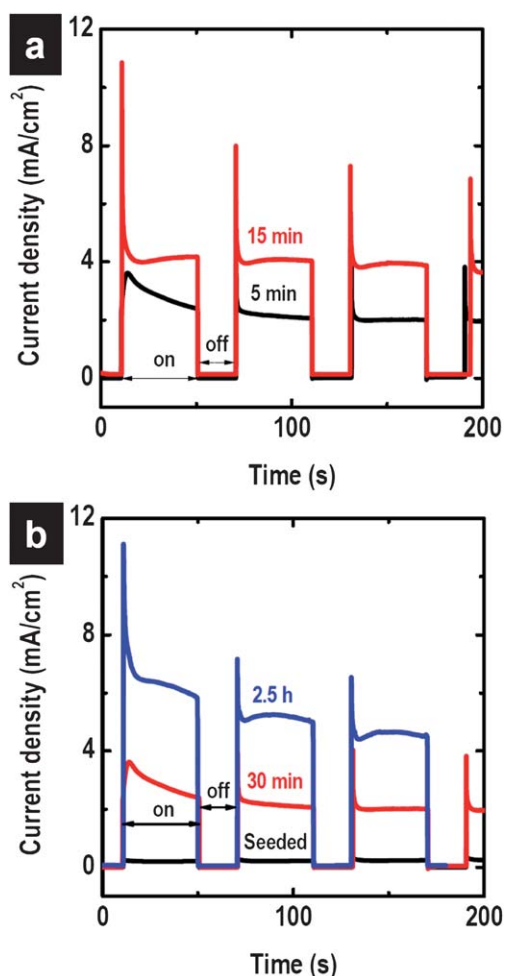
Fig. 4 Steady state current density *vs.* external bias (*J–V*) on (a) 30 min growth of ZnO NW branches on Si NW arrays from various etching times (5 and 15 min) and (b) ZnO NW branches grown for varying times on 5 min etched Si NW arrays. Insets show the dark current of corresponding samples. (C) Optical image of a 3D branched NW photoelectrode: (left) in the dark and (right) H₂ gas evolution under illumination.

electrodes compared to the core–shell Si/ZnO NW sample (Si NWs are coated with the seeding ZnO layer). The photocurrent density increases with the length of ZnO NW branches, which reaches 8 mA cm^{-2} at −1.5 V for the electrode with ZnO NW

branches grown for 2.5 h, which is about twice and 80 times compared to that for electrodes with ZnO NW branches of 30 min growth and ZnO coated Si NW electrodes, respectively. This enhancement in the photocurrent for photoelectrodes with longer and wider ZnO branches is probably due to the increase in the surface reaction area, which dominates the deficiency in reduced light absorption due to scattering (Fig. 3a and b). The superior current density levels achieved here are mainly due to the heterojunction that promotes the separation of photoinduced charge carriers, as well as the much enlarged surface area for efficient reaction. The inset compares the dark current of 5 min etched Si NWs coated with the ZnO seeding layer, ZnO NWs grown for 30 min and 2.5 h, which shows a clear trend of increase in current with the increase in ZnO NW growth time and the surface area. Note in Fig. 4, anodic current was observed both in the dark and under light illumination. The anodic currents in Fig. 4a and the inset (red curves) are most likely due to the band bending at the ZnO NW surface which leads to injection of thermal and photo-induced holes from ZnO to electrolytes, which increase as the Si NWs are longer and the surface area are larger. A similar increase of anodic dark and photo-currents in Fig. 4b and the inset (red curves) is due to the surface area increase for electrodes with 30 min ZnO NW branches compared to that with ZnO seeding layer alone. However, the anodic dark and photo-currents were suppressed for electrodes with longer ZnO NW branches (Fig. 4b blue curve), which is probably due to the increase of the ZnO NW diameter further leading to less charge separation to the surface.[62,63]

In addition, the transient photocurrent (*J–t*) test of the branched heterostructural samples was carried out under intermittent light illumination and constant external bias (−1.5 V *vs.* Ag/AgCl RE), as shown in Fig. 5a and b. The dark current of polished Si is almost zero, which is negligible and consistent with previously reported data. The photocurrent density at −1.5 V of the polished p-type Si photocathode was about 0.012 mA cm^{-2} under illumination. Si NW array and branched heterostructure array electrodes increased the photocurrent density by 250 and 400 times compared to the polished p-type Si photocathode, respectively, despite the small difference from sample to sample for the Si NW array and branched heterostructure array. Si and branched heterostructure NW arrays increased the surface area and thus the surface states, which result in increased dark currents of 7.5 and 25 times compared to that of the polished Si substrate, respectively.[14] The polished p-Si photoelectrode sample did not show significant photocurrent for H₂ evolution, because of the low kinetics for H₂ evolution.[43,64] It was pointed out that the H₂ generation rate is low at large values of photovoltage, due to the competing e$^-$/h$^+$ recombination at the surface. Conversion efficiency is limited by this competing process. Kinetics for reduction of H₂O is so poor that little or no current for H₂O reduction occurs until E_f is more negative than the H$^+$/H₂ potential.[12,43,64]

One can observe a large cathodic current jump responding to the illumination due to the photo-induced electron–hole pair separation. This photocurrent decayed quickly until reaching the steady state due to the recombination of electrons and holes *via* surface and interface states. Moreover, due to the limitation of the seeding process particularly non-uniformity on the longer Si NWs, this recombination may be partially caused by the

Fig. 5 Transient current density (*J–t*) study on (a) 30 min growth of ZnO NW branches on Si NW arrays from various etching times (5 and 15 min) and (b) ZnO NW branches grown for varying times on 5 min etched Si NW arrays. These were measured at the external bias of −1.5 V (*vs.* Ag/AgCl RE).

exposure of Si NWs to the electrolytes and also accumulation at the ZnO/electrolyte interface due to surface band bending. Seeded Si NW array showed minimum dark and photocurrent response compared to the branched Si NW samples, which confirmed that the passivation of Si NW surface states using un-doped ZnO seeding layer results in the ignorable recombination and consequently low dark current. Therefore, an increase in the dark current and cathodic current overshot were mainly due to the recombination at the ZnO NW/solution interface. Note that uniform seeding layer coating was obtained on 5 min etched Si NW array leaving minimum Si NW exposure to the solution. The photoelectrochemical stability of ZnO NW|planar Si photo-cathodes was studied and significant degradation and even complete removal were noticed in acidic and basic solutions after about 1 hour. Coating of metal thin films (for example ~5 nm Pt) as a co-catalyst on ZnO photoelectrodes showed improved stability and minimized the cathodic decomposition, in addition to the strongly improved electrochemical hydrogen reduction kinetics.[65]

Conclusions

In summary, we report the synthesis of 3D ZnO/Si branched NW arrays using the low-cost solution etching/synthesis method and the utilization as photoelectrodes in a PEC cell. The 3D nanowire heterostructures compared to ZnO NW/Si planar hetero-structures, Si NW array, and Si planar structures demonstrated large enhancement in photocathodic current density (8 mA cm⁻²) and overall hydrogen evolution kinetics. This solution-based technique for NW synthesis and heterojunction formation is inexpensive and most importantly can be scaled up to the level that would be required as a primary energy production method in the near future.

Notes and references

1 C. A. Grimes, O. K. Varghese and S. Ranjan, *Light, Water, Hydrogen-the Solar Generation of Hydrogen by Water Photoelectrolysis*, Springer, University Park, PA, 2008.
2 J. Hill, E. Nelson, D. Tilman, S. Polasky and D. Tiffany, *Proc. Natl. Acad. Sci. U. S. A.*, 2006, **103**, 11206–11210.
3 S. J. Davis, K. Caldeira and H. D. Matthews, *Science*, 2010, **329**, 1330–1333.
4 M. I. Hoffert, *Science*, 2010, **329**, 1292–1294.
5 R. Agrawal, N. R. Singh, F. H. Ribeiro and W. N. Delgass, *Proc. Natl. Acad. Sci. U. S. A.*, 2007, **104**, 4828–4833.
6 N. S. Lewis, *Science*, 2007, **315**, 798–801.
7 http://en.wikipedia.org/wiki/Electrolysis_of_water.
8 J. A. Turner, *Presented in Part at the DOE Hydrogen, Fuel Cells & Infrastructure Technologies Program Review, 2004*, 2004.
9 M. Grätzel, *Nature*, 2001, **414**, 338–344.
10 A. Heller, *Science*, 1984, **223**, 1141–1148.
11 Y. Li and J. Z. Zhang, *Laser Photonics Rev.*, 2010, **4**, 517.
12 D. C. Bookbinder, J. A. Bruce, R. N. Dominey, N. S. Lewis and M. S. Wrighton, *Proc. Natl. Acad. Sci. U. S. A.*, 1980, **77**, 6280–6284.
13 S. W. Boettcher, J. M. Spurgeon, M. C. Putnam, E. L. Warren, D. B. Turner-Evans, M. D. Kelzenberg, J. R. Maiolo, H. A. Atwater and N. S. Lewis, *Science*, 2010, **327**, 185–187.
14 A. P. Goodey, S. M. Eichfeld, K.-K. Lew, J. M. Redwing and T. E. Mallouk, *J. Am. Chem. Soc.*, 2007, **129**, 12344–12345.
15 Y. W. Chen, J. D. Prange, S. Dühnen, Y. Park, M. Gunji, C. E. D. Chidsey and P. C. McIntyre, *Nat. Mater.*, 2011, **10**, 539–544.
16 M. Szklarczyk and J. O. M. Bockris, *J. Phys. Chem.*, 1984, **88**, 5241–5245.
17 R. L. Woo, R. Xiao, Y. Kobayashi, L. Gao, N. Goel, M. K. Hudait, T. E. Mallouk and R. F. Hicks, *Nano Lett.*, 2008, **8**, 4664–4669.
18 J. Hensel, G. Wang, Y. Li and J. Z. Zhang, *Nano Lett.*, 2010, **10**, 478–483.
19 W. Zhu, X. Liu, H. Liu, D. Tong, J. Yang and J. Peng, *J. Am. Chem. Soc.*, 2010, **132**, 12619–12626.
20 W.-T. Sun, Y. Yu, H.-Y. Pan, X.-F. Gao, Q. Chen and L.-M. Peng, *J. Am. Chem. Soc.*, 2008, **130**, 1124–1125.
21 L. Liu, J. Hensel, R. C. Fitzmorris, Y. Li and J. Z. Zhang, *J. Phys. Chem. Lett.*, 2009, **1**, 155–160.
22 S. U. M. Khan, M. Al-Shahry and W. B. Ingler, Jr, *Science*, 2002, **297**, 2243–2245.
23 A. Wolcott, W. A. Smith, T. R. Kuykendall, Y. Zhao and J. Z. Zhang, *Adv. Funct. Mater.*, 2009, **19**, 1849–1856.
24 I. Cesar, A. Kay, J. A. Gonzalez Martinez and M. Grätzel, *J. Am. Chem. Soc.*, 2006, **128**, 4582–4583.
25 A. Kay, I. Cesar and M. Grätzel, *J. Am. Chem. Soc.*, 2006, **128**, 15714–15721.
26 D. K. Zhong, J. Sun, H. Inumaru and D. R. Gamelin, *J. Am. Chem. Soc.*, 2009, **131**, 6086–6087.
27 W. Smith and Y. P. Zhao, *Catal. Commun.*, 2009, **10**, 1117–1121.
28 K. Sivula, F. L. Formal and M. Grätzel, *Chem. Mater.*, 2009, **21**, 2862–2867.
29 W. Smith and Y. Zhao, *J. Phys. Chem. C*, 2008, **112**, 19635–19641.
30 Y. Lin, S. Zhou, X. Liu, S. Sheehan and D. Wang, *J. Am. Chem. Soc.*, 2009, **131**, 2772–2773.
31 Y. J. Hwang, A. Boukai and P. Yang, *Nano Lett.*, 2008, **9**, 410–415.

32 O. Khaselev and J. A. Turner, *Science*, 1998, **280**, 425–427.
33 J. Shi, Y. Hara, C. Sun, M. A. Anderson and X. Wang, *Nano Lett.*, 2011, **11**, 3413–3419.
34 A. Kampmann, P. Cowache, J. Vedel and D. Lincot, *J. Electroanal. Chem.*, 1995, **387**, 53–64.
35 D. Cahen, Y. W. Chen, R. Noufi, R. Ahrenkiel, R. Matson, M. Tomkiewicz and W.-M. Shen, *Sol. Cells*, 1986, **16**, 529–548.
36 E. Garnett and P. Yang, *Nano Lett.*, 2010, **10**, 1082–1087.
37 L. Hu and G. Chen, *Nano Lett.*, 2007, **7**, 3249–3252.
38 K.-Q. Peng, X. Wang, L. Li, X.-L. Wu and S.-T. Lee, *J. Am. Chem. Soc.*, 2010, **132**, 6872–6873.
39 B. Tian, X. Zheng, T. J. Kempa, Y. Fang, N. Yu, G. Yu, J. Huang and C. M. Lieber, *Nature*, 2007, **449**, 885–889.
40 J. Zhu, Z. Yu, G. F. Burkhard, C.-M. Hsu, S. T. Connor, Y. Xu, Q. Wang, M. McGehee, S. Fan and Y. Cui, *Nano Lett.*, 2008, **9**, 279–282.
41 M. D. Kelzenberg, S. W. Boettcher, J. A. Petykiewicz, D. B. Turner-Evans, M. C. Putnam, E. L. Warren, J. M. Spurgeon, R. M. Briggs, N. S. Lewis and H. A. Atwater, *Nat. Mater.*, 2010, **9**, 239–244.
42 G. Yuan, H. Zhao, X. Liu, Z. S. Hasanali, Z. Yan, A. Levine and D. Wang, *Angew. Chem., Int. Ed.*, 2009, **48**, 9680–9684.
43 A. B. Bocarsly, D. C. Bookbinder, R. N. Dominey, N. S. Lewis and M. S. Wrighton, *J. Am. Chem. Soc.*, 1980, **102**, 3683–3688.
44 R. N. Dominey, N. S. Lewis, J. A. Bruce, D. C. Bookbinder and M. S. Wrighton, *J. Am. Chem. Soc.*, 1982, **104**, 467–482.
45 K.-Q. Peng, Y. J. Yan, S. P. Gao and J. Zhu, *Adv. Mater.*, 2002, **14**, 1164–1167.
46 K. Peng, Y. Yan, S. Gao and J. Zhu, *Adv. Funct. Mater.*, 2003, **13**, 127–132.
47 K. Peng, Y. Wu, H. Fang, X. Zhong, Y. Xu and J. Zhu, *Angew. Chem., Int. Ed.*, 2005, **44**, 2737–2742.
48 L. E. Greene, M. Law, J. Goldberger, F. Kim, C. J. Justin, Y. Zhang, R. J. Saykally and P. Yang, *Angew. Chem., Int. Ed.*, 2003, **42**, 3031–3034.
49 L. Vayssieres, *Adv. Mater.*, 2003, **15**, 464–466.
50 A. Furube, Z.-S. Wang, K. Sunahara, K. Hara, R. Katoh and M. Tachiya, *J. Am. Chem. Soc.*, 2010, **132**, 6614–6615.
51 K. Sun, Y. Jing, N. Park, C. Li, Y. Bando and D. Wang, *J. Am. Chem. Soc.*, 2010, **132**, 15465–15467.
52 D. D. D. Ma, C. S. Lee, F. C. K. Au, S. Y. Tong and S. T. Lee, *Science*, 2003, **299**, 1874–1877.
53 S. Dengyuan and G. Baozeng, *J. Phys. D: Appl. Phys.*, 2009, **42**, 025103.
54 Y. S. Choi, J. Y. Lee, W. H. Choi, H. W. Yeom and S. Im, *Jpn. J. Appl. Phys.*, 2002, **41**, 7357.
55 Y. Cui, Z. Zhong, D. Wang, W. U. Wang and C. M. Lieber, *Nano Lett.*, 2003, **3**, 149–152.
56 L. Rayleigh, *Proc. London Math. Soc.*, 1879, **s1-11**, 51–56.
57 Y.-F. Huang, S. Chattopadhyay, Y.-J. Jen, C.-Y. Peng, T.-A. Liu, Y.-K. Hsu, C.-L. Pan, H.-C. Lo, C.-H. Hsu, Y.-H. Chang, C.-S. Lee, K.-H. Chen and L.-C. Chen, *Nat. Nanotechnol.*, 2007, **2**, 770–774.
58 X. W. Sun and H. S. Kwok, *J. Appl. Phys.*, 1999, **86**, 408–411.
59 A. Djurišić and Y. H. Leung, *Small*, 2006, **2**, 944–961.
60 M. A. Green and M. J. Keevers, *Progr. Photovolt.: Res. Appl.*, 1995, **3**, 189–192.
61 K. Sun, A. Kargar, N. Park, K. N. Madsen, P. W. Naughton, T. Bright, Y. Jing and D. Wang, *IEEE J. Sel. Top. Quantum Electron.*, 2011, **17**, 1033–1049.
62 C. Soci, A. Zhang, B. Xiang, S. A. Dayeh, D. P. R. Aplin, J. Park, X. Bao, Y.-H. Lo and D. Wang, *Nano Lett.*, 2007, **7**, 1003–1009.
63 C. Soci, A. Zhang, X. Bao, H. Kim, Y. Lo and D. Wang, *J. Nanosci. Nanotechnol.*, 2010, **10**, 1430.
64 D. C. Bookbinder, N. S. Lewis, M. G. Bradley, A. B. Bocarsly and M. S. Wrighton, *J. Am. Chem. Soc.*, 1979, **101**, 7721–7723.
65 K. Sun, K. Madsen, P. Andersen, W. Bao, Z. Sun and D. Wang, *J. Nanotechnol.*, 2012, submitted.